Visualization of the movement of single histidine kinase molecules in live *Caulobacter* cells

J. Deich*†, E. M. Judd†‡§, H. H. McAdams‡, and W. E. Moerner*¶

Departments of *Chemistry and §Applied Physics, Stanford University, Stanford, CA 94305; and ‡Department of Developmental Biology, Stanford University School of Medicine, Stanford, CA 94305

Edited by Robin M. Hochstrasser, University of Pennsylvania, Philadelphia, PA, and approved October 4, 2004 (received for review June 11, 2004)

The bacterium *Caulobacter crescentus* divides asymmetrically as part of its normal life cycle. This asymmetry is regulated in part by the membrane-bound histidine kinase PleC, which localizes to one pole of the cell at specific times in the cell cycle. Here, we track single copies of PleC labeled with enhanced yellow fluorescent protein (EYFP) in the membrane of live *Caulobacter* cells over a time scale of seconds. In addition to the expected molecules immobilized at one cell pole, we observed molecules moving throughout the cell membrane. By tracking the positions of these molecules for several seconds, we determined a diffusion coefficient (*D*) of 12 ± 2 × 10^{-3} $\mu m^2/s$ for the mobile copies of PleC not bound at the cell pole. This *D* value is maintained across all cell cycle stages. We observe a reduced *D* at poles containing localized PleC-EYFP; otherwise *D* is independent of the position of the diffusing molecule within the bacterium. We did not detect any directional bias in the motion of the PleC-EYFP molecules, implying that the molecules are not being actively transported.

single molecule | diffusion | PleC | enhanced yellow fluorescent protein

The inner membranes of bacterial cells contain proteins required for a wide variety of functions, including energy generation, solute transport, signaling, proteolysis, polar morphogenesis, chemotaxis, and cell division (1–3). The size of the diffusion coefficient (*D*) of these proteins in the membrane can affect their interactions with each other and with cytoplasmic proteins. For example, in *Escherichia coli*, the MinCDE system for locating the division plane is thought to require a difference in *D* between the membrane-associated and the cytoplasmic forms of the MinD and MinE proteins for its proper function (4–6). The *D* values of several cytoplasmic proteins have been measured in *E. coli* (7). Measurements of *D* for membrane proteins in eukaryotic cells, using fluorescence recovery after photobleaching (FRAP) (8), single gold bead tracking (9–11), and single-molecule tracking techniques (12, 13), have yielded values ranging from 5 × 10^{-3} to 500 × 10^{-3} $\mu m^2/s$.

Each *Caulobacter* cell division produces a pair of distinct daughter cells (Fig. 1): a motile swarmer (SW) cell with a single flagellum located at a specific pole and a stalked (ST) cell possessing an adhesive holdfast at the end of the stalk, allowing it to attach to a surface (14, 15). The transmembrane histidine kinase PleC regulates polar organelle formation, motility, and asymmetric cell division in *Caulobacter* (16). PleC is a 90-kDa inner membrane protein, with four predicted transmembrane domains as obtained from TMPRED (www.ch.embnet.org/software/TMPRED_form.html). Cells with mutant PleC do not form stalks or pili and have paralyzed flagella (17–19). These mutant cells undergo symmetric cell division, producing two daughter cells of similar size, each possessing a paralyzed flagellum. By using conventional fluorescence microscopy, molecules of PleC were found to be localized to the flagellar pole of SW and predivisional (PD) cells (20) (Fig. 1). Three mechanisms have been proposed for this localization: (*i*) diffusion and capture, in which PleC molecules diffuse freely throughout the inner membrane until they arrive at a binding site at the pole, at which point they are captured (21, 22); (*ii*) directed insertion, in which PleC molecules are inserted into the inner membrane at the pole as they are translated (23, 24); and (*iii*) active transport, in which PleC molecules are actively moved to the pole by a motor protein.

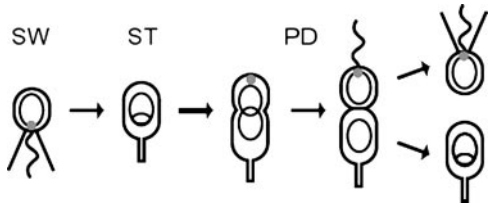

Fig. 1. *Caulobacter crescentus* cell cycle. The motile SW cell has a polar flagellum (wavy line) and pili (straight lines) and does not replicate its DNA (nonreplicating DNA represented as a ring). The PleC protein (gray dot) is localized to the flagellar pole of the SW cell. During differentiation into a ST cell, the flagellum is shed and a stalk is built at the same pole, DNA replication initiates (θ structure), and localized PleC is no longer visible. After the ST cell develops into a PD cell, PleC localizes to the new flagellar pole. The PD cell divides to yield a SW cell and a ST cell.

We used single-molecule fluorescence microscopy to observe the motion of PleC molecules tagged with the enhanced yellow fluorescent protein (EYFP) in living cells. A strain of *Caulobacter* expressing the inner membrane protein PleC fused to EYFP from the chromosome, under the control of the PleC promoter, was constructed to observe the location and movement of single PleC-EYFP molecules. Although many PleC-EYFP molecules are indeed found localized to the flagellar pole of SW or PD cells, the sensitivity of the technique enabled the detection of single molecules of PleC-EYFP diffusing in all parts of the membrane. We determined *D* by tracking the PleC-EYFP molecules for several seconds. Single-molecule imaging (25, 26) avoids some of the complications of fluorescence recovery after photobleaching without the perturbations imposed by the tracking of large beads.

The genetically encoded autofluorescent protein EYFP enables labeling PleC in living cells, while avoiding complications arising from the use of extrinsic dyes. EYFP is an order-of-magnitude easier to detect than membrane-permeable biarsenical dyes such as fluorescein arsenical helix binder (FlAsH) (27). EYFP has a high quantum yield, is relatively photostable when compared with other fluorescent proteins, is monomeric, and its optimal excitation is at a longer wavelength than enhanced GFP, thus reducing autofluorescence. Limitations of EYFP as a label in single-molecule experiments (28) include blinking, a higher quantum yield of photobleaching, and a lower overall brightness

This paper was submitted directly (Track II) to the PNAS office.

Abbreviations: D, diffusion coefficient; EYFP, enhanced yellow fluorescent protein; DF, darkfield; MSD, mean square displacement; SW, swarmer; ST, stalked; PD, predivisional.

†J.D. and E.M.J. contributed equally to this work.

¶To whom correspondence should be addressed. E-mail: moerner@stanford.edu.

than many organic dye fluorophores. However, EYFP proved sufficiently robust for single-molecule diffusion measurements.

A variety of autofluorescent proteins (29–31) have been used in single-molecule experiments in live eukaryotic cells (12, 32), by using optical techniques broadly applicable to a range of systems (33). Other single-molecule experiments in eukaryotic cells have used chemically labeled proteins and peptides to observe motion in the extracytoplasmic leaflet of the plasma membrane (13, 34), but this technique cannot address questions about the interior of a bacterium. Single-molecule fluorescence experiments in live bacteria (35) have been limited by the small size of the cells (relative to the diffraction limited spatial resolution), as well as by the presence of cellular autofluorescence (primarily from various flavinoids) that can obscure the desired signal (36). Single proteins have also been tracked in bacteria by attaching them to polystyrene beads (37), but the large size of the beads (relative to the protein studied) makes them likely to perturb the motion of the protein.

Materials and Methods

Bacterial Strains and Plasmids. Strain EJ148 contains a C-terminal fragment of PleC fused to EYFP (BD Biosciences), integrated into the chromosome at the PleC locus. This integration results in full-length PleC-EYFP expression under the control of the PleC promoter, as well as a C-terminal fragment of PleC that is not under the control of the PleC promoter. EJ148 was made by φCR30 phage transduction (38) of the PleC-EYFP allele from strain LS3205 (20) into CB15N, a synchronizable derivative of the wild-type strain CB15. Strain EJ153 contains EYFP under the control of the xylose promoter (39), integrated into the chromosome at the xylose locus so that soluble (cytoplasmic) EYFP protein is produced in the presence of xylose.

Sample Preparation. *Caulobacter crescentus* strains were grown overnight in peptone–yeast extract (PYE) complex media (38) at 30°C. An aliquot was removed, and the cells were washed and resuspended in M2G minimal media (38), and then incubated until the A_{660} reached ≈0.4. An aliquot of these cells was harvested, washed twice, and spread on a pad (18 mm × 18 mm × ≈0.5 mm) of 2% agarose (Sigma, A-0169) in M2G minimal media, mounted on a 25-mm × 75-mm glass slide. The cells grew and divided on the slides, and data collection lasted no more than 2 h on each slide. Viability at 2 h was verified by showing that cultures could be grown from small agarose pad pieces bearing the bacteria.

E. coli DH10B cells expressing high levels of EYFP protein from the pEYFP plasmid (BD Biosciences) were washed twice and then resuspended in PBS buffer (40). After sonication, unbroken cells and cell membranes were separated from the cytoplasmic contents by centrifugation. The cytoplasmic fraction was diluted and mixed with a molten (37°C) 1.5% (wt/vol) agarose/M2G solution. The liquid agarose was sandwiched between two coverslips and allowed to cool to room temperature to create a solid slab of agarose containing EYFP protein.

Microscopy. Darkfield (DF) and epifluorescence images were acquired by using a Nikon TE300 inverted microscope. A Nikon S-Fluor ×100 oil immersion objective with a numerical aperture that can be varied between 0.5 and 1.3 was used to collect both types of images. Images were recorded with a Roper Scientific (Trenton, NJ) PentaMAX intensified charge-coupled device (ICCD) camera. Calibration experiments using a 1951 U.S. Air Force test pattern (Edmund Industrial Optics, Barrington, NJ) demonstrated that each pixel on the camera corresponded to a 53 ± 1-nm square in the focal plane of the sample.

For epifluorescence microscopy, illumination was provided by the 514-nm line of a Coherent Innova 200 argon ion laser, coupled through a polarization-preserving single mode fiber (Oz Optics, Carp, ON, Canada). A $\lambda/4$ wave plate was used to convert the linearly polarized output of the fiber into circularly polarized light, to average out most effects of chromophore orientation. A 40-cm focal length lens was placed 2.5 cm from the back of the microscope to expand the area of illumination at the plane of the sample to a Gaussian spot with a full-width-half-maximum (FWHM) size of 10 μm, and a peak intensity of 2.1 kW/cm^2. All single-molecule fluorescence signals were filtered through a 525DRLP dichroic beamsplitter (XF2030, Omega Optical, Brattleboro, VT), a 530EFLP emission filter (XF105, Omega Optical), and a 514-nm notch filter (HNPF-514.5-1.5, Kaiser Optical Systems, Ann Arbor, MI). This collection of optimized filters was essential to allow observation of single EYFP molecules in the bacterial cell.

To allow the slowly moving molecules to move a significant and easily measured distance while maintaining a record of their position, we implemented time-lapse imaging by placing a variable delay between the 100-ms exposures. During the time that the camera was not recording, the laser's illumination was shuttered to limit photobleaching. A variety of time delays between 100-ms exposures was investigated, including delays of 0, 0.9, and 14.9 seconds. For D measurements, all images were acquired at 1-s intervals. No movement of the *Caulobacter* cells was visible over time scales much longer than those used in these experiments.

DF Image Processing. DF images were analyzed by using MATLAB (Mathworks, Natick, MA). A brightness histogram was computed for each image and fit to a sum of two Gaussians, resulting from the intensity contributions of the background and the cells respectively. The threshold was chosen to be 4 standard deviations above the mean of the background Gaussian. A binary image was created in which all pixels with intensity above the threshold had a value one, and all other pixels had a value zero. By using this binary image, the midpoint and two endpoints of each cell were located, and the cell midline was approximated as a half-ellipse fit to these three points. The midline was used to assign normalized positions to single-molecule trajectories (see below). Cells were excluded from further analysis if they were not completely within the image or if their measured area fell below 0.4 μm^2, the size of the smallest cell in a set of 100 measured. Each cell in the binary images was assigned a cell type by visual inspection of morphology, coupled with the existence or absence of localized fluorescence from PleC-EYFP at the cell's flagellar pole. Neither the flagellum nor the stalk is visible in the DF images, but the combination of the cell shape and the pattern of PleC-EYFP fluorescence was sufficient to categorize the cells. Swarmer cells are short, are uncurved, are unpinched, and possess localized PleC-EYFP at one pole. ST cells are unpinched and lack polarly localized PleC-EYFP. PD cells are longer than SW cells, are curved, possess a pinched region near their center, and have localized PleC-EYFP at one pole. Finally, all binary images were visually inspected to assure that the objects detected were the correct size and shape to be *Caulobacter* cells.

Fluorescence Image Processing. To obtain single-molecule position trajectories, the center location of each fluorescent molecule was recorded for each frame to the nearest pixel by visual inspection, and trajectories were terminated when the molecule disappeared due to photobleaching or moved out of focus. Every trajectory tracked was confirmed to be within the borders of a cell located in the corresponding DF image. In addition, if fluorescent spots collided or approached other fluorescent spots, thus confusing their identity across consecutive frames, they were not tracked. Finally, fluorescent spots immobilized at flagellar poles were not analyzed.

EYFP has a significant quantum yield of photobleaching, Φ_B, in live cells [$\Phi_B = 2.0 \times 10^{-5}$ to 3.8×10^{-5} in human embryonic

kidney (HEK) cells] (31), and thus the observation period was limited for each molecule at the intensities required for the experiment. A *Caulobacter* cell is ≈430 nm thick (41), slightly larger than the setup's depth of focus (≈350 nm), and molecules sometimes moved out of focus during observation. Drift of the microscope also caused the entire cell to move out of focus occasionally. All of these effects limited the time over which a single molecule could be followed. Only molecules that could be tracked for at least three frames were included in a calculation of the planar mean square displacement (MSD). Molecules were pooled as appropriate (see below).

Simulations. We simulated 2D diffusion on the surface of a cell using MATLAB. The cell was modeled as a cylinder of diameter 0.5 μm and length 3 μm, capped with a half-sphere of radius 0.25 μm at each end, leading to a total cell length of 3.5 μm. In a small time interval dt (taken as 0.5 ms), each molecule moved a small distance $dl = (4 \cdot D \cdot dt)^{1/2}$ in a random direction along the simulated cell's surface. For each molecule, we chose a random initial location on the cell surface and simulated the diffusion of this molecule during time intervals ranging from 1 to 9 s. The initial and final positions of the molecule were projected onto a plane parallel to the long axis of the cell, and the distance between these projected initial and final positions was calculated. This distance corresponds to the displacement that would be observed in our imaging experiments. The effects of a finite depth of focus were not included.

For the purposes of determining the D values for PleC-EYFP, we simulated the diffusion of 2,000 molecules over a 9-s time interval, recording positions every second. From these simulations, we calculated the planar MSD for time intervals corresponding to the experiments. We repeated the simulation for different values of D until we found a value of D for each time interval that yielded the measured planar MSD.

For predicting the effect of a molecule's position within the cell on its planar MSD, we simulated 10,000 molecules over a 1-s time interval, in cells of length 3.5 μm (average of all cells), 2.4 μm (SW cells), 2.7 μm (ST cells), and 3.9 μm (PD cells). We divided the cells lengthwise into 10 bins and calculated the planar MSD for the molecules diffusing within each bin. Molecules that crossed the boundary between sections during the 1-s time interval were assigned to the section in which the midpoint of their motion fell. We repeated these simulations for different values of D until we found a value of D for each cell type and bin that yielded the measured planar MSD.

Results

Imaging of PleC-EFYP in Live Cells. We acquired fluorescence images at fixed time intervals of live *Caulobacter* cells expressing PleC-EYFP (strain EJ148) (Figs. 2*A* and 3) to characterize the motion of the PleC-EFYP molecules. The images showed the expected bright spot of several localized PleC-EYFP at the cell pole of SW and PD cells, in addition to dimmer spots from single molecules in all cell types. We also acquired a DF image of each cell (Fig. 3, first column) to determine the cell's shape and position. By using a combination of optimized filters, an intensified charge-coupled device camera, and laser illumination, we were able to detect the fluorescence from individual PleC-EYFP molecules in the images. Illumination with total photon energies similar to those used in our experiments, and at slightly shorter wavelengths, has been shown to be nontoxic to bacterial cells containing enhanced GFP (7), and we saw no evidence of toxicity due to the EYFP or the laser illumination. Therefore, we believe that the cells we imaged remained viable throughout the experiment.

Controls. We also imaged *Caulobacter* strains EJ153 (soluble EYFP, Fig. 2*B*) and CB15N (wild-type, Fig. 2*C*) under identical conditions to verify that we were observing only PleC-EYFP, and not cellular autofluorescence or soluble EYFP that had been cleaved from the PleC-EYFP fusion protein. These controls illustrate the low autofluorescence of *Caulobacter* cells under a 514-nm illumination (Fig. 2*C*) and the "blurring" caused by the rapid diffusion of soluble cytoplasmic EYFP on the 100-ms time scale of the image (Fig. 2*B*). Multiple fluorescence images taken by using the CB15N strain showed no fluorescent objects with sufficient brightness and/or frame-to-frame continuity, which could be mistaken for PleC-EYFP. Soluble EYFP protein never appears as a 240-nm-sized spot in a 100-ms exposure, due to its rapid motion. Therefore the fluorescence spots we observe are signals from the PleC-EYFP fusion protein.

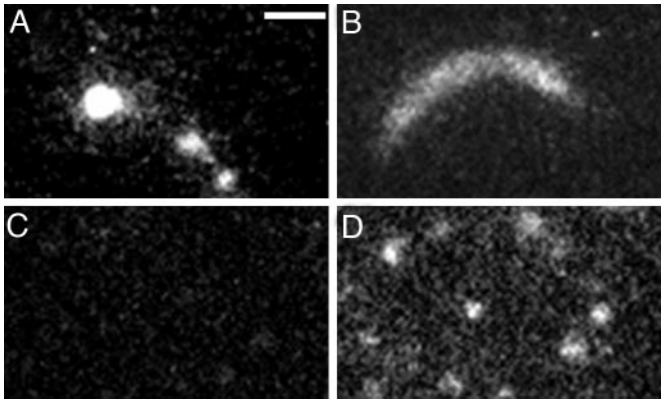

Fig. 2. Fluorescence images of three strains of *Caulobacter* and EYFP in a gel. All images are scaled by the intensity of their illumination and are displayed on an identical grey scale. (*A*) Strain EJ148, expressing PleC-EYFP. (*B*) Strain EJ153, expressing soluble, cytoplasmic EYFP. (*C*) Strain CB15N, wild-type *Caulobacter*. (*D*) EYFP molecules immobilized in an agarose gel. (Scale bar: 1 μm.)

Calibration of Single PleC-EFYP Brightness Using Gels. We confirmed the ability of our setup to detect single EYFP molecules by imaging a dilute solution of EYFP protein immobilized in an agarose gel (Fig. 2*D*). Because EYFP is relatively insensitive to its immediate environment (28, 29), we expect the number of photons detected per EYFP molecule to be similar for EYFP in agarose and PleC-EYFP in a cell. Single EYFP molecules can be easily identified because they exhibit "digital" photobleaching; they disappear in a single frame rather than gradually fading out over several frames. In addition, a single immobile EYFP molecule appears in our images as a round spot with a diameter of ≈240 nm, close to the diffraction-limited spot size. This control determines the expected fluorescence intensity of a single EYFP under our imaging conditions.

Identification of Single PleC-EYFP Molecules in Live Cells. Identification of single molecules within the *Caulobacter* fluorescence images was done by eye, and involved several criteria, including the size of the fluorescent spot, its intensity, its persistence over several consecutive frames, and the sudden or complete appearance or disappearance of emission. Although many of the molecules either appeared or disappeared in a single frame, as they did when imaged in the gels, others seemed to fade in or out over a few frames. This effect is because molecules in the cells are not immobilized and can move in and out of the focal plane, and/or drift in the microscope focus can occur. Therefore, digital photobleaching alone could not be used as the sole criterion for the presence of a single molecule, and the combined criteria described above were necessary. It is possible that some of the spots identified as single molecules are in fact due to dimers or other multimers of PleC-EYFP. For example, the top

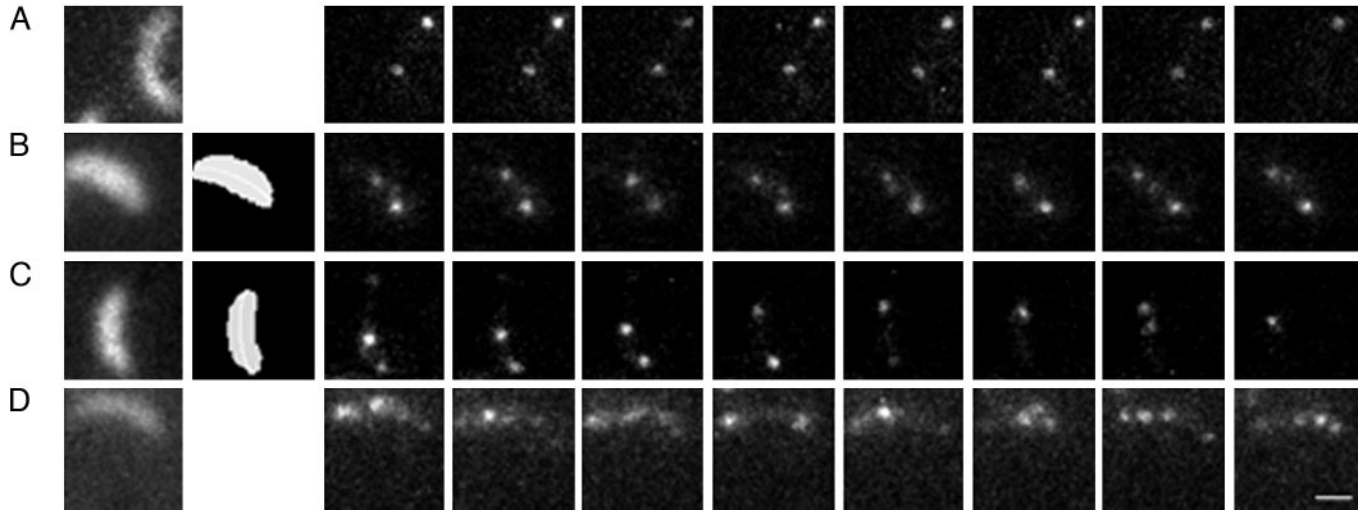

Fig. 3. Sequences of fluorescence images, spaced by three different time intervals. The leftmost image in each row is a DF image, to illustrate the orientation of the cell. The second column contains processed DF images for cells in which tracking occurred, showing the position of the cells (gray) and the computed cell midlines (white). (*A*) Images acquired every 100 ms; note the photobleaching of the lower molecule in the second to last frame. (*B* and *C*) Images acquired every 1 s. (*D*) Images acquired every 15 s. The exposure time per image in all cases is 100 ms. (Scale bar: 1 μm.)

molecule in the first three frames of Fig. 3*C* is brighter than most single molecules and shows the two-step photobleaching characteristic of a dimer. However, because we observed many cases of one-step digital photobleaching, the majority of the spots used in the analysis are expected to be due to single molecules. It is not known whether PleC forms dimers, but other bacterial histidine kinases have been shown to dimerize (42).

Caulobacter cells measure an average of 3.5 μm in length, and 0.43 μm in diameter (41), relatively small compared with the diffraction-limited spot size ($\approx$0.25 μm). Therefore, individual fluorescent molecules can be distinguished in a *Caulobacter* cell only if there are fewer than about five well-spaced molecules visible at any one time. In the initial two or three images of most sequences, too many PleC-EFYP molecules were visible to allow identification of individuals. However, in later frames, photobleaching (43) reduces the emitting population, and single molecules were easily identified. Comparing the integrated intensity of the first fluorescence image with the integrated intensity of a single EYFP in a gel, we estimate that we begin recording images with $\approx$20 molecules of PleC-EYFP visible within SW and PD cells, and fewer than 20 within ST cells.

Tracking of PleC-EYFP Molecules in Cells. Time-lapse imaging was used to follow the molecular motion and minimize photobleaching. For example, Fig. 3 shows a representative series of images taken with dark periods of 0 s (Fig. 3*A*), 0.9 s (Fig. 3 *B* and *C*), and 14.9s (Fig. 3*D*) between images. Continuous image acquisition bleaches the molecules before they have moved more than a few pixels on the intensified charge-coupled device (Fig. 3*A*). Conversely, acquiring an image every 15 s leads to confusion as to a given molecule's identity in consecutive frames; the molecule has been displaced too far, and becomes "lost" among other PleC-EYFP spots (Fig. 3*D*). All images used for the quantitative diffusion analysis described below were taken at 1-s intervals (Fig. 3 *B* and *C*).

Tracked molecules were a minimum of five pixels (265 nm) wide, in accordance with the aforementioned diffraction-limited spot size. The center position of each single molecule was recorded for each image until the molecule could no longer be tracked. PleC-EYFP that was immobilized at flagellar poles was not analyzed, because it was difficult to locate a single molecule at a pole to which PleC-EYFP is localized. We recorded the trajectories of 400 molecules from a total population of 646 cells. The average trajectory was five frames long, corresponding to 5 s. We used these trajectories to calculate the planar MSD of PleC-EYFP for time intervals or lags (Δt) of 1 to 9 seconds (Fig. 4, triangles). For example, to calculate planar MSD for $\Delta t = 3$ s, we used positions 1,4; 2,5; 3,6, etc. The major sources of error were spatial resolution and the low signal-to-noise ratio of the spots. We term this a planar MSD because the observed motion is the projection of 3D motion in the roughly cylindrical surface of the membrane onto a 2D focal plane. The long axis of the cells lies in the *x*–*y*, or image plane, and the imaging method does not detect small displacements in the *z* direction. Therefore, the actual distance moved by the molecule will be larger than the measured displacement. We refer to the true 3D MSD of the molecule as the "true MSD."

Simulation to Determine Geometrical Correction Factor. To estimate the true MSD corresponding to the measured planar MSD, we simulated diffusion on the surface of a cell, modeled as a cylinder

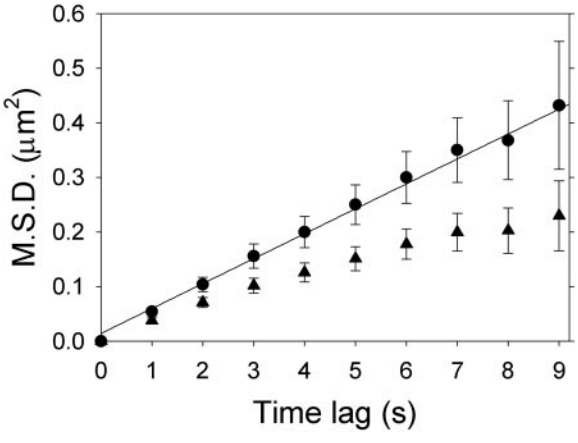

Fig. 4. MSD versus time lag for both the raw data and the data corrected for the 2D projection. Triangles represent the raw planar MSD calculated directly from trajectories. Circles denote the corresponding geometry-corrected true MSD. The fit to the corrected data has a slope of 0.049 μm^2/s, yielding a 2D diffusion coefficient D of $12 \pm 2 \times 10^{-3}$ μm^2/s.

Table 1. Two-dimensional diffusion coefficients, *D*, determined from 1-s time-lag data (*N* = 1,956) as a function of cell type and position along the cell axis

	s coordinate										
	0–0.1	0.1–0.2	0.2–0.3	0.3–0.4	0.4–0.5	0.5–0.6	0.6–0.7	0.7–0.8	0.8–0.9	0.9–1	All
All	4	12	16	19	11	17	15	16	18	14	13
SW	3		17		20		16		14		14
PD	4		16		10		16		19		12
ST	13		17		14		16		22		16

D was measured in each of 10 equal sections along the *s* coordinate. This was repeated for each subset of the population: SW, ST, and PD cells, using five bins for each subset. *D* is given in units of 10^{-3} $\mu m^2/s$, corrected for the 2D projection as described in the text. All *D* values are ±20%.

with spherical ends. A molecule was initially placed at a random location on the surface of the virtual cell and then allowed to diffuse along the 3D cell surface. The position was recorded at time intervals Δt, and a 2D trajectory was generated by projecting the motion onto the *x–y* plane, and the simulated planar MSD was computed. For each time lag, we repeated the simulation for various values of the true MSD until the simulated planar MSD equaled the measured planar MSD. We then plotted these calculated true MSD values vs. Δt (Fig. 4, circles).

The Diffusion Coefficient of PleC-EYFP. For a particle undergoing Brownian diffusion, the MSD is proportional to the time lag. Our measured planar MSD shows a sublinear dependence on Δt, i.e., the planar MSD increases more slowly with increasing Δt than would be expected for Brownian diffusion. However, the true MSD, which is corrected for the 3D geometry of the cell, is linear with Δt, within the error of our measurements. Therefore, we conclude that the PleC-EYFP molecules are undergoing Brownian diffusion on the 1- to 10-s time scale. A linear fit to the corrected data has a slope of 0.049 $\mu m^2/s$. Using $D = MSD/(4\Delta t)$ we calculate a *D* of $12 \pm 2 \times 10^{-3}$ $\mu m^2/s$. Any apparent subdiffusion caused by our positional uncertainty (53 nm) is negligible given the magnitude of *D* and the long time scale involved, as determined according to the methods of Martin *et al*. (44).

The Diffusion Coefficient of PleC-EYFP Does Not Vary with Cell Type. To investigate whether the diffusion coefficient of PleC-EYFP is different for cells at different stages of the cell cycle, we used the DF images in conjunction with the existence or absence of pole-localized PleC-EYFP to assign all of the cells to one of the three major life cycle stages of *Caulobacter*: SW, ST, or PD. For the cells in each category, we calculated the planar MSD of PleC-EYFP for Δt = 1 s, and simulated diffusion on the cell surface as above to extract values for *D*. *D* did not vary significantly for cells at different life stages (far right column, Table 1).

The Diffusion Coefficient as a Function of Position Within the Cell. To determine whether the PleC-EYFP diffusion coefficient varies with location within the cells, we created a normalized coordinate system as described in *Materials and Methods*, with *s* as a normalized coordinate along the long axis of the cell. In cells with PleC-EYFP localized to the flagellar pole (SW, PD), *s* varied from zero (at the localization site) to 1 (the opposite pole). In ST cells, where PleC is distributed symmetrically, the $s = 0$ position was arbitrarily assigned to one pole. The *s* coordinate of a molecule was taken to be the point on the s arc that was closest to the location of the molecule. We divided all of the displacement measurements into 10 sections along the *s* axis and calculated the planar MSD for each of these 10 sections for Δt = 1 s (Table 1). We also sorted the cells by cell type and then divided the categorized data into five sections along the *s* arc. Diffusion simulations were performed to determine the true MSD values corresponding to the measured planar MSD values for each length bin and cell type, as described in *Materials and Methods*. For a given value of the true MSD, the calculated planar MSD is independent of *s* except at the cell ends, where it is ≈17% smaller than in the middle of the cell. The resulting *D* values shown in Table 1 were largely independent of *s* for each cell type, except for a reduction in *D* at the flagellar pole of SW and PD cells. This reduction in *D* is probably due to the localized, immobilized molecules present at this pole. Although we attempted to avoid tracking these immobilized molecules, some may have been tracked. It is also possible that molecules that were initially mobile became immobilized at the pole during tracking, thereby reducing their MSD. Finally, the membrane's viscosity may be higher at the poles than in the rest of the cell, or the topology of the membrane at the poles may be different from that used in our model.

Motion of PleC-EFYP Is Not Biased Along the *s* Axis. We determined that molecules were equally likely to move in the $+s$ or $-s$ directions (Fig. 5); 48.4% of the observations moved in the −s direction, within the expected range (50.0 ± 2.3%, $n = 1{,}956$) for a random process with two outcomes. This result was true regardless of whether or not the cell had a localized cluster of PleC-EYFP present at the pole. Thus, despite the cell's polar asymmetry, PleC-EYFP motion is random along the *s* axis, arguing that active, directed motion is not being used to accumulate PleC-EYFP at the pole.

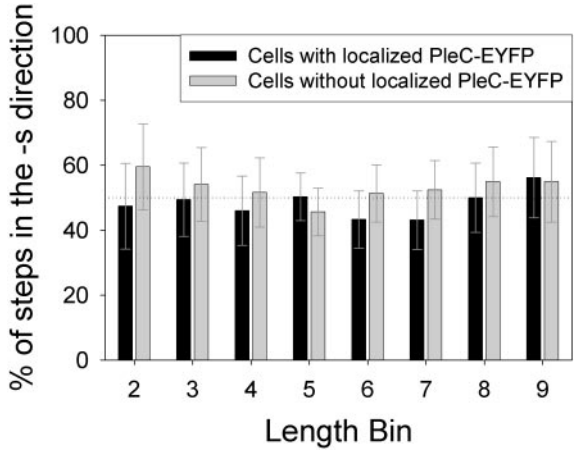

Fig. 5. Percentage of steps in the $-s$ direction. Each bin represents one tenth of the cell, divided lengthwise. In cells with localized PleC-EYFP, bin 1 includes the flagellar pole. Motion in the $-s$ direction is motion toward this pole. In cells without PleC-EYFP localization, one end is arbitrarily assigned as the first bin. Data are not shown for bins 1 or 10 because the *s* axis arc is not well aligned with the cell axis in these bins.

Discussion and Conclusions

We tracked the motion of individual PleC-EYFP molecules for time scales ranging from 100 ms through several seconds. Although a combination of photobleaching and motion in and out of the focal volume limited observations of molecular motion to 5 s on average, we measured D as a function of position within the cell and of cell cycle stage. Within the precision of our measurements, the D value for PleC-EYFP is uniform across all cell types and positions within the cell. No directional bias in the motion of PleC-EFYP was detected. The true MSD of PleC-EYFP is linear with time for the time scales assayed, as expected for Brownian diffusion. We cannot exclude the possibility that PleC-EYFP molecules display non-Brownian motion for time scales smaller than 1 s or larger than 9 s. It is possible that D for the PleC-EYFP fusion protein (mass of 117 kDa) differs somewhat from D for native PleC protein (mass of 90 kDa). However, because the PleC-EFYP protein is functional (20), any change in D or other properties does not affect the function of the protein.

Our measured D value of $12 \pm 2 \times 10^{-3}$ $\mu m^2/s$ is near the low end of the range of diffusion coefficients measured for membrane proteins in eukaryotic cells (8), including lipid-linked EYFP in human airway smooth muscle cell membranes ($110 \pm 40 \times 10^{-3}$ $\mu m^2/s$) (31), L-type Ca^{2+} channels in human embryonic kidney cell membranes ($140 \pm 50 \times 10^{-3}$ $\mu m^2/s$) (12), and glycosylphosphatidylinositol-linked (220×10^{-3} $\mu m^2/s$), and native (180×10^{-3} $\mu m^2/s$) I-E^k class II MHC proteins in the plasma membrane of Chinese hamster ovary (CHO) cells (13, 34). It is roughly 200 times smaller than the D value of $2{,}500 \pm 600 \times 10^{-3}$ $\mu m^2/s$ measured by fluorescence recovery after photobleaching for a cytoplasmic protein of similar mass (GFP fused to maltose-binding protein, 72 kDa) in *E. coli* (7). Finally, it is well below the maximum diffusion coefficient detectable with a high numerical aperture objective in 100 ms (10 $\mu m^2/s$) (45).

The D of PleC-EYFP varies little from one cell cycle stage to another and seems to be uniform throughout the *Caulobacter* inner membrane for PleC molecules not localized at a pole. Our results argue against an active transport mechanism, because we did not detect directed motion of PleC molecules. When coupled with the MSD's linearity with time (Fig. 4), this finding suggests that the motion of PleC in the membrane is governed by Brownian processes. The presence of freely diffusing PleC molecules throughout the *Caulobacter* cell membrane is consistent with the diffusion and capture mechanism of polar localization (21, 22). However, directed insertion cannot be ruled out. It is possible that most PleC molecules are inserted into the membrane at the pole, where they remain, while a few molecules are inserted elsewhere in the membrane, where they are free to diffuse. Extraction of more detailed information about the motion of proteins in future studies will rest upon the development of improved autofluorescent labels with reduced photobleaching or alternative labeling and detection methods.

W.E.M. thanks the IBM Corporation for the donation of electronic apparatus. This material is based on work supported in part by Defense Advanced Research Projects Agency Grant MDA972-00-1-0032 (to W.E.M. and H.H.M.), by National Science Foundation Grant MCB-0212503 (to W.E.M.), and by Office of Naval Research Grant N00014-02-1-0538 (to H.H.M.).

1. Kadner, R. J. (1996) in *Escherichia coli and Salmonella*, ed. Neidhardt, F. C. (Am. Soc. Microbiol., Washington, DC), Vol. 1, pp. 58–87.
2. Miller, C. G. (1996) in *Escherichia coli and Salmonella*, ed. Neidhardt, F. C. (Am. Soc. Microbiol., Washington, DC), Vol. 1, pp. 938–954.
3. Jensen, R. B., Wang, S. C. & Shapiro, L. (2002) *Nat. Rev. Mol. Cell. Biol.* **3,** 167–176.
4. Meinhardt, H. & de Boer, P. A. (2001) *Proc. Natl. Acad. Sci. USA* **98,** 14202–14207.
5. Howard, M., Rutenberg, A. D. & de Vet, S. (2001) *Phys. Rev. Lett* **87,** 278102.
6. Kruse, K. (2002) *Biophys. J.* **82,** 618–627.
7. Elowitz, M. B., Surette, M. G., Wolf, P. E., Stock, J. B. & Leibler, S. (1999) *J. Bacteriol.* **181,** 197–203.
8. Edidin, M. (1994) in *Mobility and Proximity in Biological Membranes* (CRC, Boca Raton, FL), pp. 109–135.
9. Kusumi, A., Sako, Y. & Yamamoto, M. (1993) *Biophys. J.* **65,** 2021–2040.
10. Simson, R., Sheets, E. D. & Jacobson, K. (1995) *Biophys. J.* **69,** 989–993.
11. Saxton, M. J. & Jacobson, K. (1997) *Annu. Rev. Biophys. Biomol. Struct.* **26,** 373–399.
12. Harms, G. S., Cognet, L., Lommerse, P. H. M., Blab, G. A., Kahr, H., Gamsjager, R., Spaink, H. P., Soldatov, N. M., Romanin, C. & Schmidt, T. (2001) *Biophys. J.* **81,** 2639–2646.
13. Vrljic, M., Nishimura, S. Y., Brasselet, S., Moerner, W. E. & McConnell, H. M. (2002) *Biophys. J.* **83,** 2681–2692.
14. McAdams, H. H. & Shapiro, L. (2003) *Science* **301,** 1874–1877.
15. Ausmees, N. & Jacobs-Wagner, C. (2003) *Annu. Rev. Microbiol.* **57,** 225–247.
16. Wang, S. P., Sharma, P. L., Schoenlein, P. V. & Ely, B. (1993) *Proc. Natl. Acad. Sci. USA* **90,** 630–634.
17. Sommer, J. M. & Newton, A. (1989) *J. Bacteriol.* **171,** 392–401.
18. Ely, B., Croft, R. H. & Gerardot, C. J. (1984) *Genetics* **108,** 523–532.
19. Fukuda, A., Asada, M., Koyasu, S., Yoshida, H., Yaginuma, K. & Okada, Y. (1981) *J. Bacteriol.* **145,** 559–572.
20. Wheeler, R. T. & Shapiro, L. (1999) *Mol. Cell* **4,** 683–694.
21. Shapiro, L., McAdams, H. H. & Losick, R. (2002) *Science* **298,** 1942–1946.
22. Rudner, D. & Losick, R. (2002) *Proc. Natl. Acad. Sci. USA* **99,** 8701–8706.
23. Steinhauer, J., Agha, R., Pham, T., Varga, A. W. & Goldberg, M. B. (1999) *Mol. Microbiol.* **32,** 367–377.
24. Robbins, J. R., Monack, D., McCallum, S. J., Vegas, A., Pham, E., Goldberg, M. B. & Theriot, J. A. (2001) *Mol. Microbiol.* **41,** 861–872.
25. Moerner, W. E. & Orrit, M. (1999) *Science* **283,** 1670–1676.
26. Weiss, S. (1999) *Science* **283,** 1676–1683.
27. Zhang, J., Campbell, R. E., Ting, A. Y. & Tsien, R. Y. (2002) *Nat. Rev. Mol. Cell. Biol.* **3,** 906–918.
28. Moerner, W. E. (2002) *J. Chem. Phys.* **117,** 10925–10937.
29. Tsien, R. Y. (1998) *Annu. Rev. Biochem.* **67,** 509–544.
30. Sullivan, K. F. & Kay, S. A., eds. (1999) *Methods in Cell Biology* (Academic, New York), Vol. 58.
31. Harms, G. S., Cognet, L., Lommerse, P. H., Blab, G. A. & Schmidt, T. (2001) *Biophys. J.* **80,** 2396–2408.
32. Sako, Y., Minoguchi, S. & Yanagida, T. (2000) *Nat. Cell Biol.* **2,** 168–172.
33. Moerner, W. E. & Fromm, D. P. (2003) *Rev. Sci. Instrum.* **74,** 3597–3619.
34. Vrljic, M., Nishimura, S. Y., Moerner, W. E. & McConnell, H. M. (2005) *Biophys. J.*, in press.
35. Xu, X.-H. N., Brownlow, W., Huang, S. & Chen, J. (2003) *Biochem. Biophys. Res. Commun.* **305,** 79–86.
36. Benson, R. C., Meyer, R. A., Zaruba, M. E. & McKhann, G. M. (1979) *J. Histochem. Cytochem.* **27,** 44–48.
37. Oddershede, L., Dreyer, J. K., Grego, S., Brown, S. & Berg-Sorensen, K. (2002) *Biophys. J.* **83,** 3152–3161.
38. Ely, B. (1991) *Methods Enzymol.* **204,** 372–384.
39. Meisenzahl, A. C., Shapiro, L. & Jenal, U. (1997) *J. Bacteriol.* **179,** 592–600.
40. Sambrook, J. & Russell, D. W. (2001) *Molecular Cloning* (Cold Spring Harbor Lab. Press, Plainview, NY).
41. Fukuda, A., Iba, H. & Okada, Y. (1977) *J. Bacteriol.* **131,** 280–287.
42. Stock, J. B., Surette, M. G., Levit, M. & Park, P. (1995) in *Two-Component Signal Transduction*, eds. Hoch, J. A. & Silhavy, T.J. (Am. Soc. Microbiol., Washington, DC), pp. 25–51.
43. Peterman, E. J. G., Brasselet, S. & Moerner, W. E. (1999) *J. Phys. Chem. A* **103,** 10553–10560.
44. Martin, D. S., Forstner, M. B. & Kas, J. A. (2002) *Biophys. J.* **83,** 2109–2117.
45. Kubitscheck, U. (2002) *Single Mol.* **3,** 267–274.